

VELOCITY AND Q STRUCTURE OF THE GREAT VALLEY, CALIFORNIA, BASED ON SYNTHETIC SEISMOGRAM MODELING OF SEISMIC REFRACTION DATA

BY LORRAINE J. HWANG AND WALTER D. MOONEY

ABSTRACT

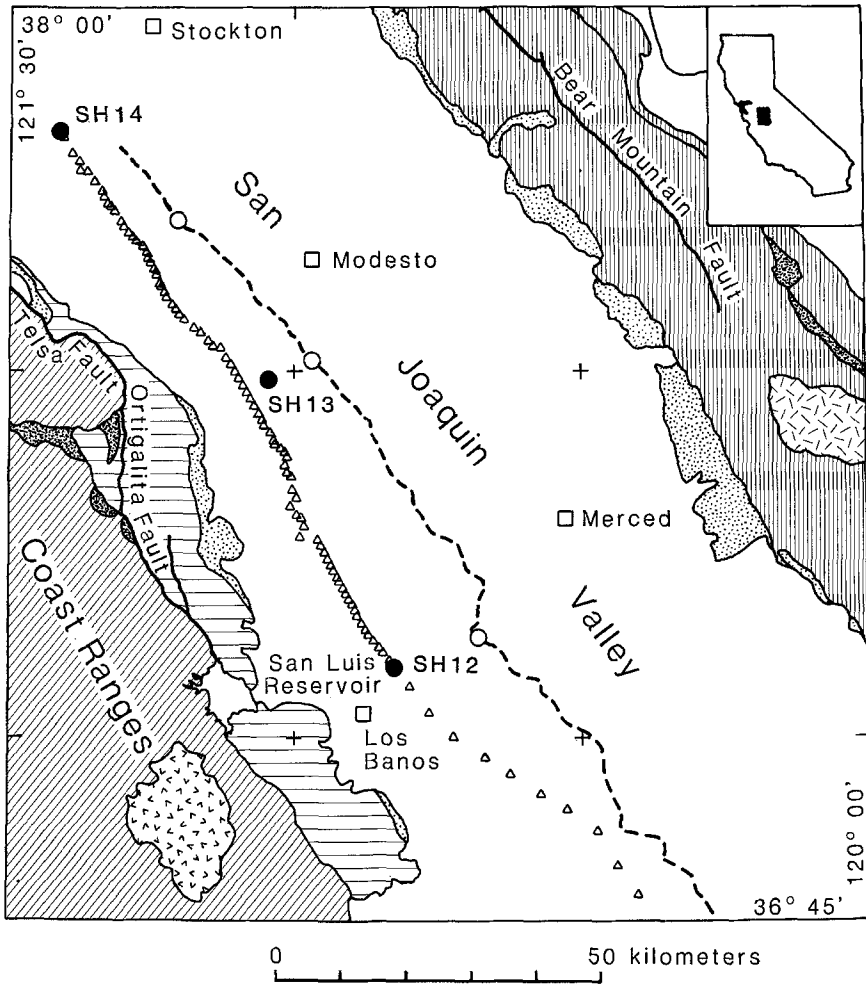
The modified reflectivity method is used here to interpret seismic refraction data from the west side of the Great Valley, California, in terms of a one-dimensional compressional wave velocity model of the crust. In addition, the apparent attenuation, Q_p , has been estimated for the 6-km-thick sedimentary section. The reflectivity method was used to calculate the prominent free-surface multiples that propagate in this sedimentary section. Modeling of the normalized amplitudes of these multiples yielded average Q_p values of 100 from 0 to 2.83 km depth and 200 from 2.93 to 6.20 km depth. The velocity structure in the crust is complicated. It is characterized by positive velocity gradients within the sediment to a depth of 4.8 km and by a 1.4-km-thick, low-velocity zone below this depth. The sediment overlies a basement with a velocity of 5.7 km/sec at its top, which increases to 6.3 km/sec at 12 km depth. Ambiguity of the data in critical regions leads to two equally valid interpretations of the lower crust at depths of 16 to 27 km: simple step increases or a more complex structure consisting of alternating high- and low-velocity zones.

INTRODUCTION

The Great Valley of central California is a 700-km-long and 100-km-wide northwest-trending asymmetric sedimentary basin (Figure 1). The Valley is bordered to the east by the Sierra Nevada and to the west by the Coast Ranges. The basin is filled with a thick sequence of relatively undeformed Jurassic through Recent sediments and underlain by a westward-dipping crystalline basement.

The Great Valley has long been an exploration target for oil and gas, and much is known about the structure and composition of the Valley sediments from seismic reflection and drill hole data. However, relatively little is known about the structure and composition of the crystalline crust beneath the Valley, which has only recently been investigated with modern seismic methods. Earlier investigations include two seismic refraction profiles shot in the early 1960s across the Valley from San Francisco to Fallon, Nevada (Eaton, 1963; 1966; Prodehl, 1979) and from San Luis Obispo to the Nevada Test Site (Prodehl, 1979). Each of these profiles included only 12 recording points in the Valley; there were no shot points within the Valley itself. The large travel-time delays observed at the Valley stations confirmed the presence of a great thickness of sediments in the Valley, but the data were insufficient to define the velocity structure of the sediments in detail or to constrain the deeper crustal structure. Some inferences concerning the deeper structure can be obtained from potential field data. Cady (1975) presented detailed models of the structure across the Valley based on gravity and magnetic modeling. In his preferred model, sialic crust is nonexistent beneath the Great Valley, and gabbroic rocks (oceanic crust) account for the large gravity and magnetic anomalies.

In October 1981, the U.S. Geological Survey conducted a seismic refraction survey along the west side of the Valley (Figure 1), where drill hole data indicate approximately 6 km of sediments. One hundred vertical-component seismographs were deployed along a northwest-southeast-trending profile paralleling the approximate



EXPLANATION

- | | |
|--------------------------------|-----------------------------|
| Quaternary Sedimentary Rocks | Ultramafic Rocks |
| Tertiary Sedimentary Rocks | Granitic Rocks |
| Tertiary Volcanic Rocks | Mesozoic Metamorphic Rocks |
| Mesozoic Great Valley Sequence | Seismograph location |
| Franciscan Assemblage | Shot point |
| | Parallel refraction profile |

FIG. 1. Generalized geologic map (after Jennings, 1977) showing the location of the western Great Valley (San Joaquin Valley), California, seismic refraction profile. Note that SH13 is offset 4 km northeast of the nearest recorder on the western profile. Southeast of SH12, the station spacing increases to 5 km, and the trend of the line is more easterly. The data from SH14 only are analyzed here.

trend of the Valley. Along the northern portion of this 150 km profile, station spacing averaged about 1 km and increased to 5 km along the southern end. Three shots were fired: (1) shot 14 (SH14) at the northernmost end; (2) shot 13 (SH13) 50 km southeast of SH14 and displaced approximately 4 km east of the line; and

(3) shot 12 (SH12) 46 km northwest of the southernmost section. Since SH13 was displaced east of the recording profile, a fully reversed profile was recorded only between SH12 and SH14.

INTERPRETATION METHOD

Seismic refraction profiles are often interpreted mainly on the basis of the travel times of refractions and the wide-angle reflections. For reversed profiles, a two-dimensional velocity model may be obtained by trial-and-error ray trace modeling of these phases (e.g., Mooney *et al.*, 1983; Fuis *et al.*, 1984). Amplitudes may be incorporated into the interpretation procedure by the calculation of ray theoretical synthetic seismograms (e.g., Červený *et al.*, 1977; McMechan and Mooney, 1980). However, with ray theory synthetic seismograms, it is difficult to include all possible phases, such as converted waves and free-surface multiples. In addition, losses due to attenuation are usually not considered with ray methods. In the present study, we use the reflectivity synthetic seismogram method (Fuchs and Müller, 1971; Kind, 1978; 1979) to model seismic refraction data. Although the method is restricted to one-dimensional models (i.e., planar layers), we prefer to use this method because we seek to model all of the phases evident in our profiles (particularly free-surface multiple refractions), and to estimate the attenuation structure of the sedimentary section as well. Modeling of the data in terms of two-dimensional velocity structure will be presented elsewhere (Colburn and Mooney, 1986; Holbrook and Mooney, 1986).

DATA

Figure 2 shows the data collected along the profile. The data for the three shots are very similar; the seismic phases that dominate these record sections are the secondary phases A2, A3, A4, and WG. These prominent secondary phases are free-surface multiples which have refracted in the high-velocity gradient of the sediments and have been reflected at the surface one or more times. Phase A2 has undergone a single free-surface reflection and has refracted in the sediments twice; phase A3 has undergone two reflections, and has refracted three times, etc. (Figure 3). Similar phases were also observed in a refraction survey of the Imperial Valley in southern California, and their travel-time and amplitude behavior are discussed in McMechan and Mooney (1980) and Fuis *et al.* (1984). WG denotes the "whispering gallery" phase that propagates just below the free surface. This phase includes both very high-order, free-surface multiple reflections and the direct arrival (Hill *et al.*, 1982). Hence, the envelope of the whispering gallery phase travels at the surface *P*-wave velocity.

Another clear secondary phase, phase B1, has a low apparent velocity suggesting that it could be a *P-S* converted phase. This phase appears most clearly in SH14 (Figure 2A). Like phases A2 to A4, phase B1 multiply reflects at the free surface. The multiple phase B2 can be identified in all three data sets, but the triple reflection is weak and unidentifiable for SH12 and SH13 as opposed to the strong reflection B3 for SH14. Other clear secondary phases seen on the longer record sections include the primary wide-angle reflections C, D, and E (Figure 2).

The travel times of all observed phases at any given range for SH12 and SH14 differ by at most 0.4 sec and generally agree within 0.2 sec. This agreement, as well as the ability to match phases between sections, indicates that the assumption of lateral homogeneity in the velocity structure inherent in the application of the modified reflectivity method is valid. Since the record sections are very similar,

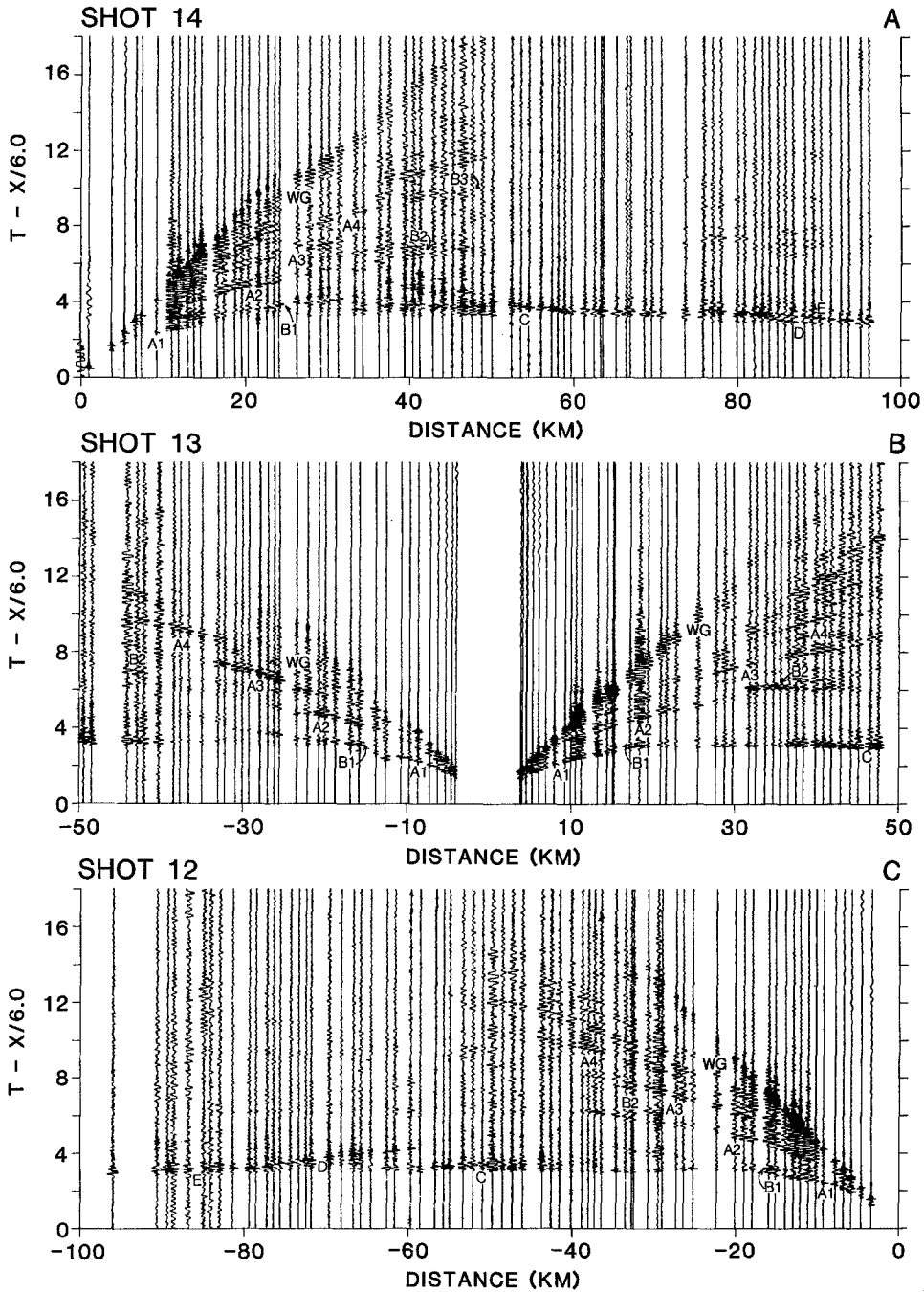
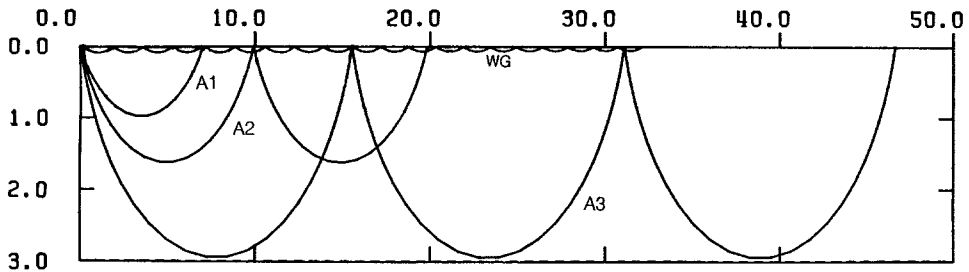


FIG. 2. Seismic record sections for the three shots (Figure 1). Amplitudes of all traces are normalized. Data south of SH12 are not shown here. (A) SH14. A1: first arrivals refracted in the sediments. A2, A3, and A4: free-surface multiples of A1 which have reflected from the surface and refracted in the sediments 2 to 4 times, respectively. WG: whispering gallery phase which includes both the direct *P* wave as well as very high-order free-surface multiples which propagate just below the surface. B1: reflection off basement. B2 and B3: free-surface multiples of B1. C, D, and E: wide-angle reflections from the lower crust. (B) SH13. Labels the same as (A). (C) SH12. Labels the same as (A).

only SH14 will be modeled in this study. SH14 has the best signal-to-noise ratio, and all multiples can be clearly identified. In addition, the 1 km station spacing in the distance range of 80 to 95 km for SH14 provides the best resolution of the deep crustal structure.

ANALYSIS

The first step in synthetic seismogram modeling using the reflectivity method is to construct a good one-dimensional velocity model. The initial model is calculated, using standard equations, from slowness-offset parameters to yield homogeneous velocity layers and thicknesses. This model is then improved by trial-and-error fitting of the travel-time data using a rapid one-dimensional ray trace algorithm. Since estimates of Q are very sensitive to changes in the velocity gradient (Hill, 1971), in this study special attention was given to the velocity structure in the sediments. The positive 0.85 km/sec/km velocity gradient in the first layer derived by the above method is consistent with the travel-time data from the reversed shots, SH12 and SH14. Various models for the deeper crust are derived for the travel-time data from only SH14, and these were evaluated with the aid of the synthetic seismograms. We initially set the S -wave velocity at $V_s = V_p/\sqrt{3}$ at all depths and $Q_p = 50$ at depths of 0 to 2.93 km, 200 from 2.93 to 9.3 km, and 300 from 9.3 to 18.0 km. S -wave velocities and Q values are discussed in the following sections. Table 1 lists the model parameters for all synthetics in this paper.



SEDIMENT GRADIENT .85 KM/S/KM

FIG. 3. Ray diagram for the multiple refractions in the first layer. Phases labeled as in Figure 2.

SYNTHETIC MODELING

Whispering gallery phase. The first series of synthetic seismograms were calculated to model only the upper crust. This includes the free-surface multiple phases A2 to A4, WG, and B1 to B3 (Figure 2). The observed data (Figure 4A) are compared to the synthetic seismograms for the initial velocity model, model 1A (Figure 4B). The data and the synthetics differ in several respects. The biggest discrepancy is that the envelope of the whispering gallery phase, WG, has a group velocity of about 1.0 km/sec in the synthetic, but 1.6 km/sec (the surficial P -wave velocity) in the data. In calculating this model only, a V_p/V_s ratio of $\sqrt{3}$ was assumed throughout the crust. This yields a V_s at the surface of 0.95 km/sec, about the same as the group velocity of the synthetic whispering gallery phase. Thus, we conclude P -to- S converted phases are responsible for the low group velocity of the whispering gallery phase in the synthetic of Figure 4B. The discrepancy between data and synthetic seismograms suggests that a constant V_p/V_s ratio is not valid throughout the crust.

Actual measurements of S -wave velocity in the Great Valley place the surficial S -wave velocity at approximately 0.2 km/sec (Fumal *et al.*, 1982). Therefore, we revised the input model by using $V_s = 0.20$ km/sec at the surface and allowed the velocity to increase to 0.90 km/sec at a depth of 2.93 km. Below this depth, $V_s = V_p/\sqrt{3}$. In the resultant synthetic (model 1B, Figure 4C), the slowest apparent

TABLE 1
INPUT PARAMETERS FOR MODELS*

Model	Depth (km)	Velocity (km/sec)	Q_p
1A	0.00-2.93	1.60 (0.97)-4.10 (2.33)	50
	2.93-6.80	4.25-5.00	200
	6.80-9.30	5.50-6.50	200
	9.30-18.00	6.05-6.80	300
1B	0.00-2.93	1.60 (0.20)-4.10 (2.30)	50
	2.93-6.80	4.25-5.00	200
	6.80-9.30	5.50-6.05	200
	9.30-18.00	6.05-6.80	300
2A	0.00-2.93	1.60 (0.20)-4.10 (2.30)	50
	2.93-4.80	4.25-4.40	200
	4.80-6.20	4.23	200
	6.20-8.00	5.70-5.95	200
	8.00-12.10	5.95-6.30	200
2B	0.00-2.93	1.60 (0.20)-4.10 (2.30)	200
	2.93-4.80	4.25-4.40	200
	4.80-6.20	4.23	200
	6.20-8.00	5.70-5.95	200
	8.00-12.10	5.95-6.30	200
2C	0.00-0.20	1.60 (0.20)-1.77 (2.32)	100
	0.20-2.93	1.77-4.10	200
	2.93-4.80	4.25-4.40	200
	4.80-6.20	4.23	200
	6.20-8.00	5.70-5.95	200
	8.00-12.10	5.95-6.30	200
2D	0.00-2.93	1.60 (0.20)-4.10 (2.30)	100
	2.93-4.80	4.25-4.40	200
	4.80-6.20	4.23	200
	6.20-8.00	5.70-5.95	200
	8.00-12.10	5.95-6.30	200
3A	0.00-2.93	1.60 (0.20)-4.10 (2.30)	100
	2.93-4.80	4.25-4.40	200
	4.80-6.20	4.23	200
	6.20-8.00	5.70-5.95	200
	8.00-12.10	5.95-6.30	200
	12.10-16.30	6.30-6.43	200
	16.30-21.30	7.00	300
	21.30-27.15	7.37	300
	27.15-	7.97	300
3B	0.00-2.93	1.60 (0.20)-4.10 (2.30)	100
	2.93-4.80	4.25-4.40	200
	4.80-6.20	4.23	200
	6.20-8.00	5.70-5.95	200
	8.00-12.10	5.95-6.30	200
	12.10-16.40	6.30	200
	16.40-18.00	7.06	300
	18.00-19.70	6.90	300
	19.70-22.00	7.40-7.30	300
	22.00-26.80	7.30	300
	26.80-	7.80	300

* S -wave velocity in the first layer is in parentheses; otherwise $V_s = V_p/\sqrt{3}$. $Q_s = 0.5 Q_p$.

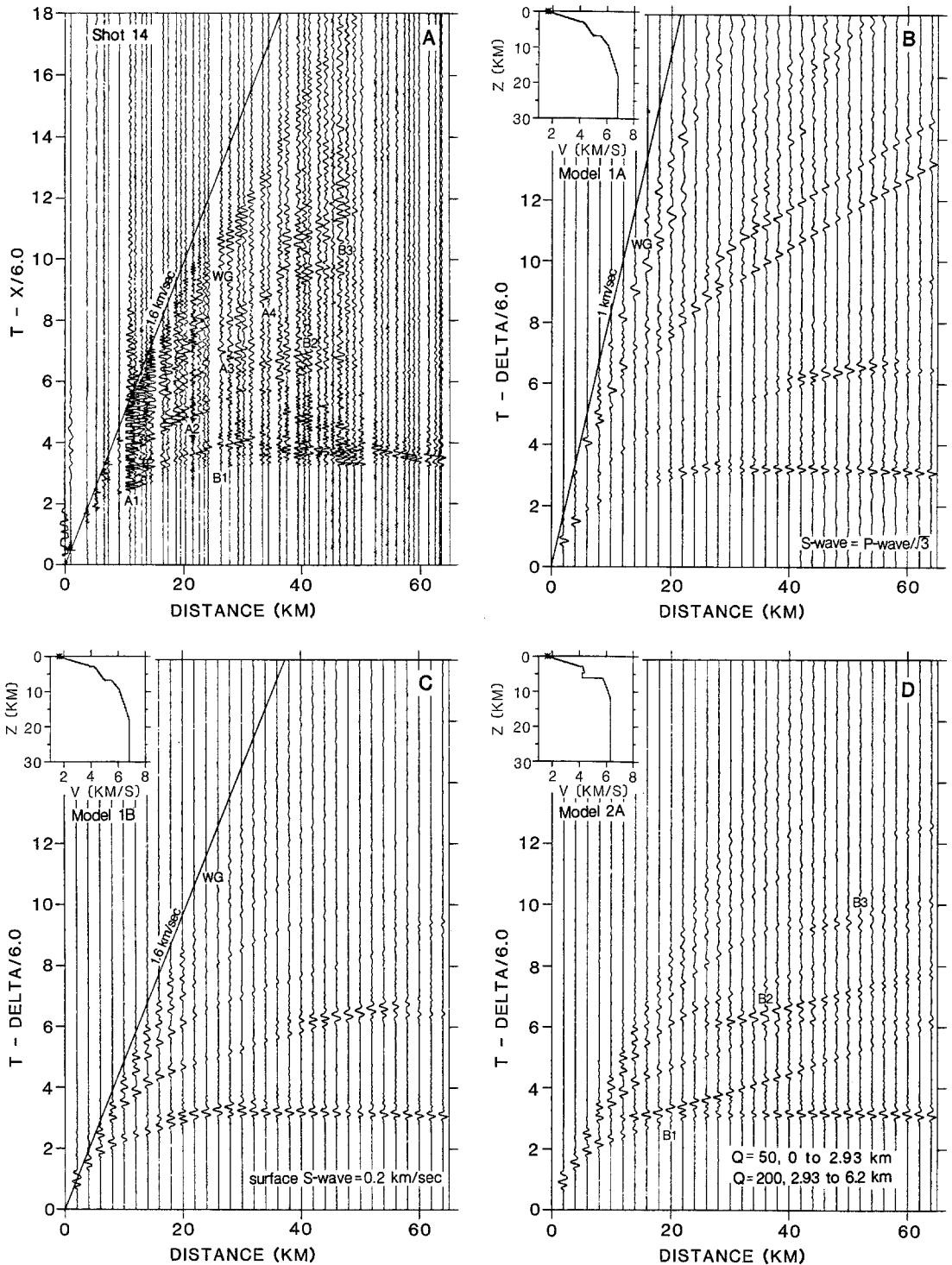


FIG. 4. Observed and synthetic record sections for SH14. The synthetic record sections in this figure and Figures 6 and 7 are plotted with a 0.2-sec positive shift relative to the data and the geometrical travel time of the velocity-depth model. For all synthetics, amplitudes are trace-normalized and Q_s , the S-wave attenuation, is assigned as one half of Q_p , the P-wave attenuation (hereafter referred to as Q). For the following models, $Q = 50$ in the first layer. Below 2.93 km, $V_s = V_p/\sqrt{3}$. All velocity-depth models are listed in Table 1. See Figure 2 for explanation of labeled phases. (A) Data from SH14. (B) Model 1A. Envelope of whispering gallery phase is traveling at approximately 1 km/sec. At the surface, $V_s = V_p/\sqrt{3}$. Velocity-depth function appears in the upper left-hand corner. (C) Model 1B. Using a lower S-wave velocity at the surface, $V_s = 0.20$ km/sec, the envelope of the whispering gallery phase now travels at approximately 1.6 km/sec as seen in the data. Notice that the travel times for B1 are too early in this model. (D) Model 2A. At the surface, $V_s = 0.20$ km/sec. Adding a low-velocity zone at the bottom of the first layer delays the reflection B1 and its multiples B2 and B3. Amplitudes of A3, A4, and WG and the signal between all phases are too low.

phase now travels at approximately 1.6 km/sec (model 1B, Figure 4C), corresponding to the whispering gallery phase WG as seen on the actual data (Figure 4A). Comparison of Figures 4B and 4C illustrates how large a change the choice of the surficial *S*-wave velocity makes in the synthetic. In particular, the amplitudes of the prominent phase between 30 and 60 km (at a reduced time of 8 to 14 sec) have been greatly reduced in Figure 4C.

We next turn to modeling the lower sediments. Before adjusting the amplitudes of the multiple phases A2 to A4 and WG, the velocity model should be adjusted to match phase B1 (Figure 4A) which occurs in the same distance range as the above phases.

Lower sedimentary section. The prominent phase B1, initially believed to possibly be a converted phase, is not matched in the synthetics for models 1A or 1B. To adequately explain the amplitudes and delayed travel times of this phase, a 1.4-km-thick, low-velocity zone was added at the bottom of the second layer (at a depth of 4.8 km). Velocity inversions within the Great Valley sedimentary column have also been reported by Walter (1985) for east-west seismic refraction profiles in the southern Great Valley 80 km south of our study area.

The resultant synthetic (model 2A, Figure 4D) is in reasonably good agreement with the data in the first 50 km. The basement reflection, phase B1, has been well-matched as have the arrival times of its multiples B2 and B3. However, amplitudes of the high-order multiple refractions from within the sedimentary column (phase WG) are too low with respect to phases B1, B2, and B3.

*Attenuation (*Q*) modeling of the sedimentary section.* The synthetic seismograms in Figure 4 were calculated with an assumed $Q = 50$ in the uppermost sedimentary layer (0 to 2.93 km). This value is apparently too low because the synthetic amplitudes of the phases A2, A3, A4, and WG relative to phases B1, B2, and B3 are weaker in the synthetic than those observed in the data (c.f. Figure 4, A and D and Figure 5A). In addition, the low Q value has attenuated the intralayer (peg-leg) multiples, yielding a very low signal strength between the free-surface multiples.

The value of Q was raised to 200 (model 2B, Figure 6B) in the depth range 0 to 2.93 km for the next calculation. In this case, the high-order multiple phases emerging from the whispering gallery phases are too strong, particularly at reduced travel times greater than 12 sec. These higher order multiples cannot be as clearly distinguished in the data. The amplitude ratios between phases A2 to A4 and WG and phases B1 to B3 have improved but are still incorrect (Figure 5B). Phases B1 to B3 are now overwhelmed by the amplitudes of phases A3, A4, the higher order multiples, and WG (Figure 6B). Clearly, an average Q of 200 for the first 2.93 km is too high.

In order to improve the fit to the data, we consider a somewhat more complex Q model in which Q does not remain constant over the depth range 0 to 2.93 km. Studies in water-saturated marine sediments show that Q depends strongly on sand content and does not necessarily increase with depth (Tullos and Reid, 1969). Trying a more complex Q model, $Q = 100$ to a depth of 200 m and $Q = 200$ for the remainder of the first layer shows that this complex Q structure cannot explain the data (model 2C, Figure 6C). Amplitude ratios between the low-order multiples are correct (Figure 5C) but the higher order multiples included in WG (i.e., at reduced times greater than 10 sec) are too energetic, and the waveforms become more complex than the data. Other arrivals, most notably B1 through B3, are correspondingly scaled down.

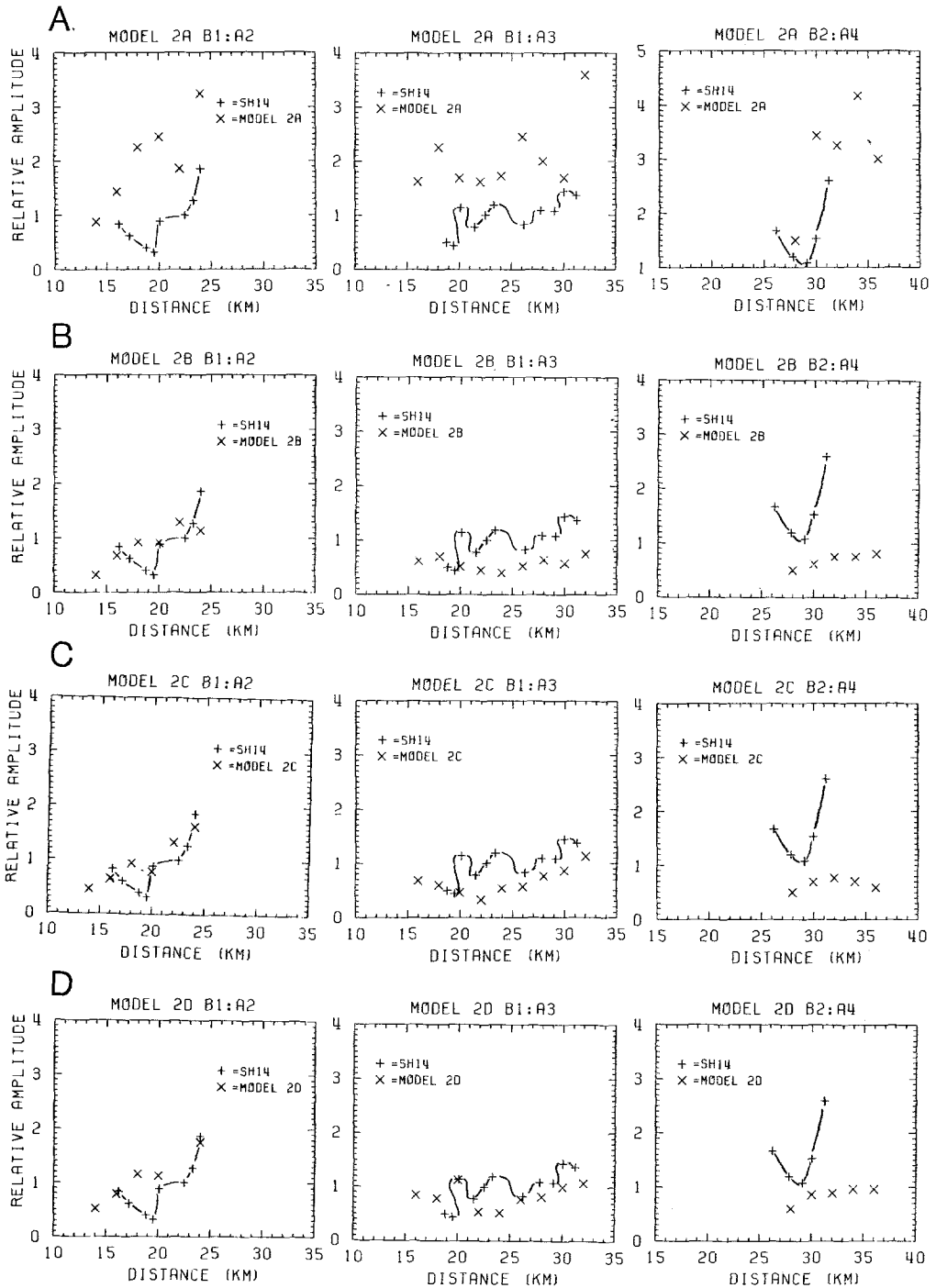


FIG. 5. Comparison of observed (+) and synthetic seismograms (x) amplitude ratios for phase B1:A2, B1:A3, and B2:A4 (c.f. Figure 4). See Figure 2 for an explanation of phases. (A) Model 2A: the low $Q = 50$ in this model attenuates the multiples A2 to A4 too rapidly with respect to the reflected arrivals B1 to B4. (B) Model 2B: the higher $Q = 200$ successfully predicts the amplitude ratios in (1) but underestimates the amplitude ratios in (2) and (3), as well as WG in Figure 6B. (C) Model 2C: a thin $Q = 100$ layer improves the fit in (1), (2) and (3). However, the amplitudes of the higher order multiples and WG (Figure 6C) overwhelm these lower order multiples. (D) Model 2D: increasing the thickness of the $Q = 100$ layer improves the amplitude ratios in (1), (2), and (3) as well as for the higher order multiples and WG in Figure 6D.

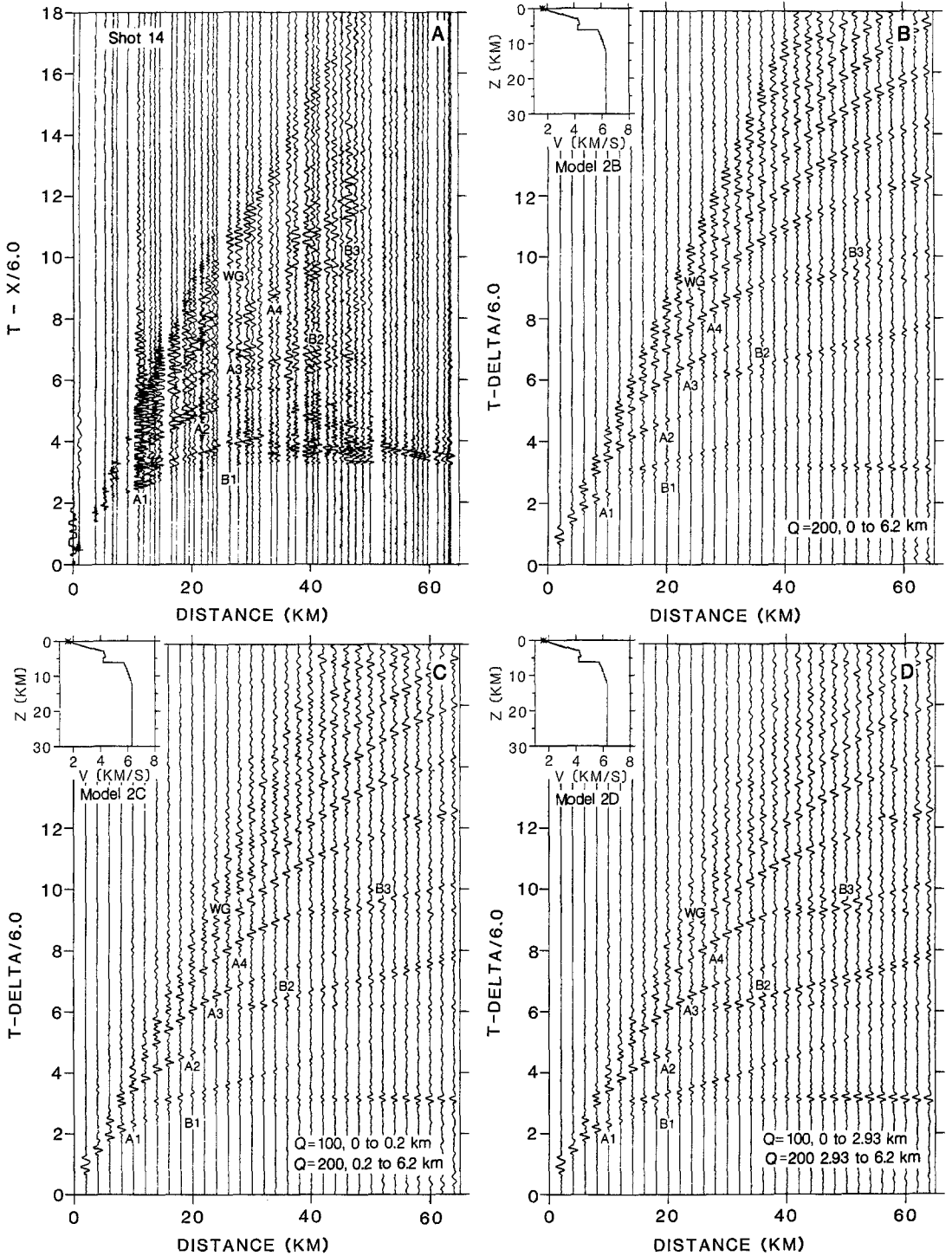


FIG. 6. Observed and synthetic record sections for SH14. Phases labeled as in Figure 2. (A) Data from SH14. (B) Model 2B: $Q = 200$ in the first layer, 0 to 2.93 km. The amplitude of WG is too large in this model and higher order multiples corresponding to more than four free-surface reflections form distinct arrivals not apparent in the data. (C) Model 2C: $Q = 100$ from 0 to 200 m and $Q = 200$ from 0.2 to 2.93 km. WG amplitudes are again too high, and relative amplitudes between WG and B1 to B3 are incorrect. Signal-to-noise ratio between multiples has now decreased. (D) Model 2D: $Q = 100$ in the first layer. Assuming a homogeneous Q in this region gives a better relative amplitude match to the data.

Assuming an intermediate Q value and a homogeneous Q structure, model 2D (Figure 6D) assigns $Q = 100$ to the first layer. In the resultant synthetic section, the whispering gallery phase WG which samples the shallower portion of the sediments is less energetic than before and the very high-order multiples have become less distinct. The amplitude ratios between all multiples are also now more consistent with the data, and the normalized amplitudes are comparable to the observed data (Figures 5D and 6A).

Lower crust. The velocity structure of the lower crust is best constrained by the wide-angle reflections (phases C, D, and E; Figure 7A). Data quality is good to a

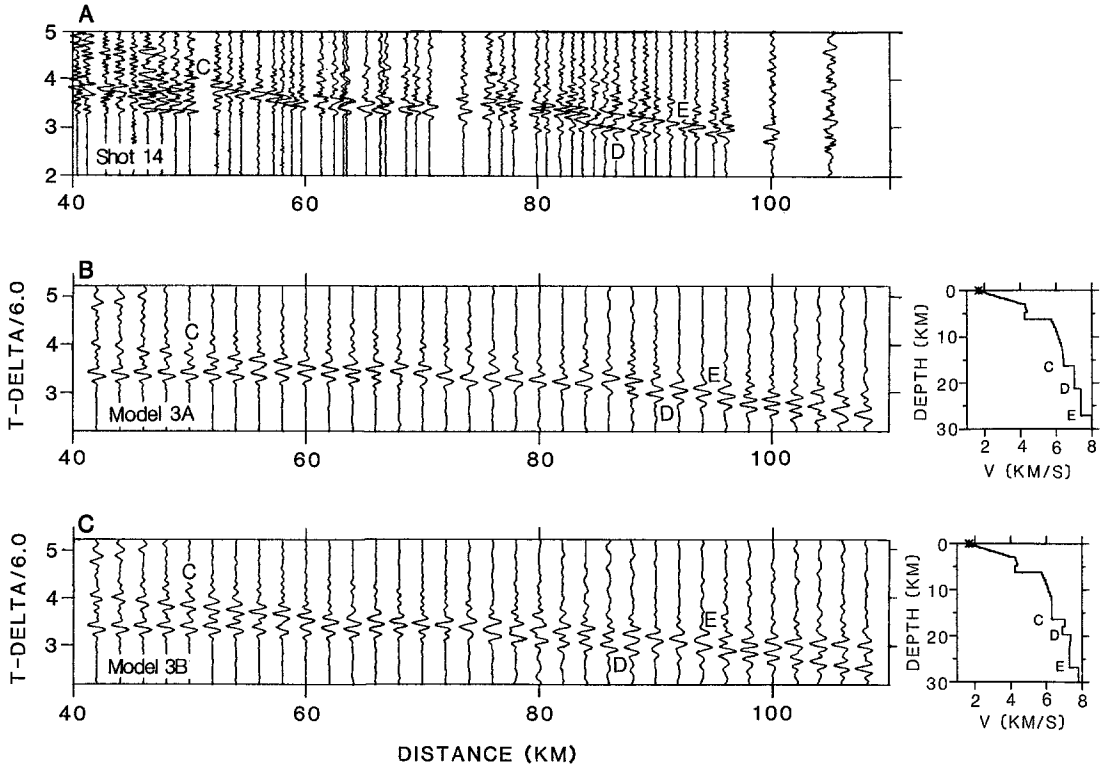


FIG. 7. Observed and synthetic record sections for a distance of 40 to 100 km corresponding to arrivals from the lower crust. (A) Data from SH14. (B) Model 3A: simple step model for the lower crust. (C) Model 3B: complex model of alternating high- and low-velocity zones for the lower crust. Note the more complex waveforms predicted by this model in contrast to model 3A. Similarities between the models and the data are too strong to rule either of them out as a possible model for the lower crust.

distance range of 100 km, but unfortunately, the wide station spacing beyond 100 km distance (Figure 1) makes it difficult to accurately determine the travel times and amplitude behavior of these phases beyond 100 km. The data between 75 to 100 km by itself does not allow an unambiguous interpretation of the structure of the lower crust and the crust-mantle transition zone. Two interpretations of the lower crust are presented here: (1) simple steps—model 3A (Figure 7B) and (2) alternating high- and low-velocity zones—model 3B (Figure 7C). Q was arbitrarily assigned a value of 300 for the lower crust (depth greater than 16.3 km).

In both models, phase C is interpreted as a reflection from a velocity step at a depth of approximately 16 km. In the synthetics, C appears as a clear secondary arrival between 45 to 60 km. A clear separation of the first and second arrivals in

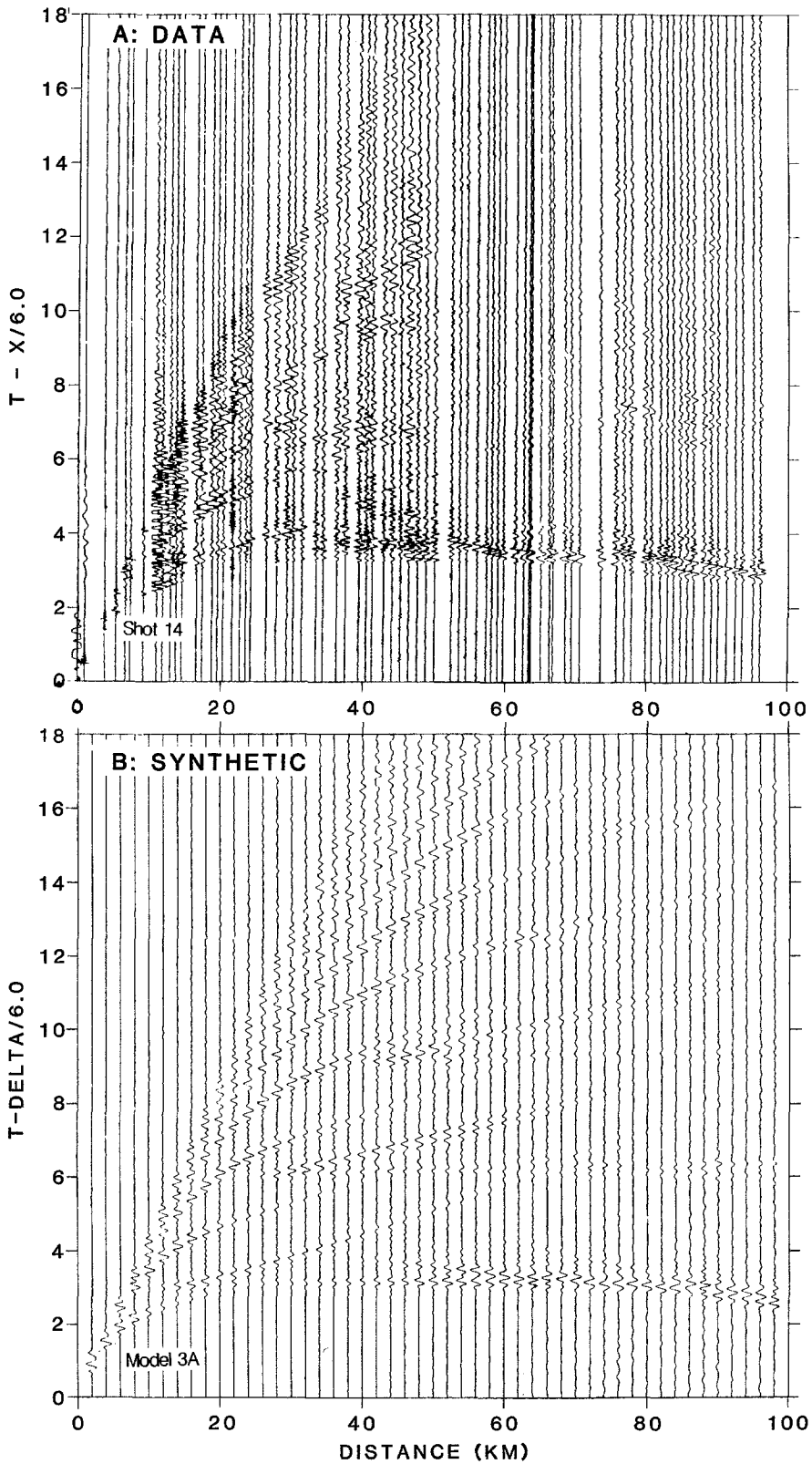


FIG. 8. (A) Seismic record section for SH14. (B). Complete synthetic seismogram section for model 3A. The pattern of the free-surface multiples as well as the wide-angle reflections have been replicated, thus explaining the major features in the data.

the data does not occur in the distance range of 45 to 50 km because of the high-amplitude coda from the first arrivals. In the data, the amplitudes of these first arrivals between 45 to 50 km have approximately the same amplitude as phase C. Model 3A predicts much larger amplitude ratios in contrast to model 3B which predicts amplitudes ratios near unity. Thus, the above amplitude feature is matched best by model 3B. However, neither model adequately matches the apparent die-off of the first arrival branch in the distance 50 to 60 km. This die-off could be explained by a small negative gradient above reflector C, but this possibility has not been explored here.

In the data (Figure 7A), phases D and E can be seen as two distinct arrivals. This feature is seen in both models 3A and 3B (Figure 7, B and C). In model 3A, phases D and E are interpreted as reflections from the top of each velocity step. In model 3B, they are interpreted as delayed reflections from the bottom of low-velocity zones, and the waveforms for that of model 3B are somewhat more complex than model 3A. For example, at 80 km, model 3A predicts phase D as a single sharp pulse and a very low-amplitude coda, but in model 3B, phase D is seen as an emerging double pulse, and phase E is a reflection of comparable amplitude. This is very similar to the data in which phase D appears as an emergent double pulse and phase E a high-amplitude secondary arrival.

Except for the above-mentioned differences, both models provide good matches to the data. While model 3B provides a closer fit to the data in some regions, model 3A cannot be ruled out. Model 3B is more complex, and hence produces more complex waveforms which tend to match the data better than simpler waveforms. However, phases C, D, and E are seen in both models, and in most regions, the synthetics for both models fit the data remarkably well. For example, between 65 to 70 km and 90 to 100 km, both models provide an almost perfect fit with the data. Thus, both one-dimensional models must be considered as reasonable approximations to the actual velocity structure. The complete observed and synthetic (model 3A) record sections are displayed in Figure 8.

CONCLUSIONS

Application of synthetic seismogram modeling of seismic refraction data from the Great Valley, central California, reveals a complex one-dimensional velocity structure. The first layer (2.93 km thick) has a high-velocity gradient from velocities of $V_p = 1.6$ km/sec and $V_s = 0.2$ km/sec to velocities of 4.1 km/sec and 0.90 km/sec, respectively. Trial and error Q modeling suggests $Q_p = 100$ in the first 2.93 km of sediments, and $Q_p = 200$ from 2.93 to 6.2 km (the lower sedimentary section). These estimates are of apparent Q ; the effects of scattering have not been excluded. Q has not been evaluated in the subsedimentary crust.

The second layer, from 2.93 to 4.8 km, consists of a gradient from 4.25 to 4.40 km/sec. It is truncated by a low-velocity zone which extends from a depth of 4.8 to 6.2 km and has a velocity of 4.23 km/sec. Modeling ruled out the interpretation of phase B, a prominent secondary arrival, as a multiple or converted phase. It is well matched in the synthetic seismograms as a delayed reflection from the top of the crystalline basement.

The crystalline crust is assumed to have linear velocity gradients: between 6.2 and 8.0 km, the velocity increases from 5.70 to 5.95 km/sec, and between 8.0 and 12.1 km, it increases from 5.95 to 6.3 km/sec. The lower crust and Moho can be modeled either by simple steps or as alternating high- and low-velocity layers, depending on the travel-time and amplitude interpretation. Despite differences in

certain regions, both models are strikingly similar to the data, and neither of them can be ruled out as a possible structure for the lower crust-mantle transition zone. Future two-dimensional modeling may help to distinguish between the two different interpretations.

Some general geologic conclusions can be made from the final velocity-depth functions (models 3A and 3B, Figure 6, Table 1), bearing in mind that our one-dimensional analysis neglects dip and may therefore be in error by some 0.2 km/sec. The Mesozoic and Cenozoic sedimentary fill of the valley amounts to 6.2 km at this locality. The velocities of the underlying basement range from 5.7 to 6.3 km/sec between a depth of 6.2 and 16.3 km. These velocities are consistent with granitic and medium to high grade metamorphic rocks (as found in the foothills of the Sierra Nevada to the east), but velocities greater than 5.9 km/sec are inconsistent with rocks of the Franciscan assemblage found to the west, as presented in the preferred velocity model of Walter and Mooney (1982). We have presented two alternative models for the lower crust but in either case the velocities are greater than 6.9 km/sec in the depth range of 16.3 to 27.2 km. These velocities are consistent with mafic rocks of possible oceanic origin as proposed by Cady (1975) and others. The total crustal thickness of 27 km is somewhat thinner than the 29 to 30 km estimate of Oppenheimer and Eaton (1984). Continuing analysis of other profiles parallel and perpendicular to the profile presented here will provide additional constraints on the structure and composition of the crust of the Great Valley.

ACKNOWLEDGMENTS

We would like to thank E. L. Ambos, R. H. Colburn, W. Joyner, J. H. Luetgert, T. V. McEvelly, and G. A. McMechan for comments on an earlier draft of this paper. Many thanks to R. Kind for the synthetic seismogram code used here, and to J. H. Luetgert for software support. The efforts of the seismic field crew including A. Boken, J. Bonomolo, E. Criley, S. Gallanthine, K. Harrington, L. Hoffman, R. Kaderabek, G. Molina, V. Sutton, J. Van Schaak, and A. Walter are greatly appreciated. Comments by an anonymous reviewer were greatly appreciated and lead to the inclusion of Figure 5.

REFERENCES

- Cady, J. W. (1975). Magnetic and gravity anomalies in the Great Valley and Western Sierra Nevada metamorphic belt, California, *Geol. Soc. Am. Special Paper 168*, 56 pp.
- Červený, V., I. A. Molotov, and I. Pšenčík (1977). *Ray Method in Seismology*, Universita Karlova, Praha, 214 pp.
- Colburn, R. H. and W. D. Mooney (1986). Two-dimensional velocity structure along the synclinal axis of the Great Valley, California, *Bull. Seism. Soc. Am.* **76** (in press).
- Eaton, J. P. (1963). Crustal structure from San Francisco, California, to Eureka, Nevada, from the seismic-refraction measurements, *J. Geophys. Res.* **68**, 5789-5806.
- Eaton, J. P. (1966). Crustal structure in northern and central California from seismic evidence, in *Geology of Northern California: California Division of Mines Bull. 190*, E. H. Bailey, Editor, 419-426.
- Fuchs, K. and G. Müller (1971). Computation of synthetic seismograms with the reflectivity method and comparison with observations, *Geophys. J. R. Astr. Soc.* **23**, 417-433.
- Fuis, G. S., W. D. Mooney, J. H. Healy, G. A. McMechan, and W. J. Lutter (1984). A seismic refraction survey of the Imperial Valley region, California, *J. Geophys. Res.* **89**, 1165-1189.
- Fumal, T. E., J. F. Gibbs, and E. R. Roth (1982). *In-situ* measurements of seismic velocity at 10 strong motion accelerograph stations in central California, *U.S. Geol. Surv., Open-File Rept. 82-407*, 76 pp.
- Hill, D. P. (1971). Velocity gradients and anelasticity from crustal body wave amplitudes, *J. Geophys. Res.* **76**, 3309-3325.
- Hill, D. P., W. D. Mooney, G. S. Fuis, and A. Walter (1982). The whispering-gallery phase in deep sedimentary basins (abstract), *Earthquake Notes* **53**, 26.
- Holbrook, W. S. and W. D. Mooney (1986). The crustal structure of the Great Valley, California, from seismic refraction measurements, *Tectonophysics* (in press).
- Jennings, C. W. (1977). Geologic map of California, California Division of Mines and Geology, Sacramento, California, 1:750,000.

- Kind, R. (1978). The reflectivity method for a buried source, *J. Geophys.* **44**, 603–612.
- Kind, R. (1979). Extensions of the reflectivity method, *J. Geophys.* **45**, 373–380.
- McMechan, G. A. and W. D. Mooney (1980). Asymptotic ray theory and synthetic seismograms for laterally varying structure: theory and application to the Imperial Valley, California, *Bull. Seism. Soc. Am.* **70**, 2021–2035.
- Mooney, W. D., M. C. Andrews, A. Ginzberg, D. A. Peters, and R. M. Hamilton (1983). Crustal structure of the northern Mississippi embayment and a comparison with other continental rift zones, *Tectonophysics* **94**, 327–348.
- Oppenheimer, D. H. and J. P. Eaton (1984). Moho orientation beneath central California from regional earthquake travel times, *J. Geophys. Res.* **89**, 10,267–10,282.
- Prodehl, C. (1979). Crustal structure of the western United States, *U.S. Geol. Surv. Profess. Paper 1034*, 74 pp., 3 plates.
- Tullos, F. N. and A. C. Reid (1969). Seismic attenuation of Gulf Coast sediments, *Geophysics* **34**, 516–528.
- Walter, A. W. (1985). Velocity structure near Coalinga, California, in *Mechanics of the May 2, 1983, Coalinga, California, Earthquake*, M. J. Rymer and W. L. Ellsworth, Editors, *U.S. Geol. Surv., Open-File Rept. 85-44*, 10–18.
- Walter, A. W. and W. D. Mooney (1982). Crustal structure of the Diablo and Gabilan ranges, central California: a reinterpretation of existing data, *Bull. Seism. Soc. Am.* **72**, 1567–1590.

U.S. GEOLOGICAL SURVEY
345 MIDDLEFIELD ROAD
MS 977
MENLO PARK, CALIFORNIA 94025

Manuscript received 26 July 1985